

Coexistence of anomalous spin dynamics and weak magnetic order in a chiral trillium lattice $\text{K}_2\text{FeSn}(\text{PO}_4)_3$

J. Khatua,^{1,*} S. Krishnamoorthi,^{2,*} Changhyun Koo,¹ Gyungbin Ban,¹ Taeyun Kim,¹ Suyoung Kim,³ Yugo Oshima,⁴ Jonas A. Krieger,⁵ Thomas J. Hicken,⁵ Hubertus Luetkens,⁵ Marc Uhlarz,⁶ Eundeok Mun,³ Kyeong Jun Lee,⁷ Seo Hyoung Chang,⁷ R. Sankar,^{2,†} and Kwang-Yong Choi^{8,‡}

¹*Department of Physics, Sungkyunkwan University, Suwon 16419, Republic of Korea*

²*Institute of Physics, Academia Sinica, Taipei 11529, Taiwan*

³*Department of Physics, Simon Fraser University, Burnaby, BC V5A 1S6, Canada*

⁴*RIKEN Pioneer Research Institute, Wako, Saitama 351-0198, Japan*

⁵*PSI Center for Neutron and Muon Sciences CNM, 5232 Villigen, Switzerland*

⁶*Dresden High Magnetic Field Laboratory (HLD-EMFL),*

Helmholtz-Zentrum Dresden-Rossendorf, 01328 Dresden, Germany

⁷*Department of Physics, Chung-Ang University, Seoul 60974, Republic of Korea*

⁸*Department of Physics, Sungkyunkwan University, Suwon 16419, Republic of Korea*

(Dated: July 17, 2025)

Trillium lattices, where magnetic ions form a three-dimensional chiral network of corner-sharing equilateral triangular motifs, offer a prominent platform to explore exotic quantum states. In this work, we report ground-state properties of the $S = 5/2$ trillium lattice compound $\text{K}_2\text{FeSn}(\text{PO}_4)_3$ through thermodynamic, electron spin resonance (ESR), and muon spin relaxation (μSR) experiments. Thermodynamic and ESR measurements reveal the two-step evolution of magnetic correlations across $T^* = 11$ K, which results from an interplay between dominant antiferromagnetic Heisenberg interactions and subleading interactions. Below T^* , dc and ac magnetic susceptibilities indicate weak magnetic ordering at $T_N \approx 2$ K under low fields, which is suppressed for $\mu_0 H \geq 2$ T, consistent with a power-law dependence of magnetic specific heat at low temperatures. μSR experiments confirm the dominance of persistent spin dynamics and the absence of conventional spin freezing, supporting the subtle nature of weak magnetic ordering coexisting with spin-liquid-like fluctuations. These findings underscore the potential for realizing a classical spin-liquid ground state with exotic excitations in high-spin trillium lattice systems.

I. INTRODUCTION

Geometrically frustrated magnets are of great interest in condensed matter physics as they offer a viable platform for realizing various quantum many-body phenomena, including quantum spin liquids (QSLs), spin ices, and fractional quantum Hall liquids [1–5]. QSLs are elusive states of matter characterized by the absence of long-range magnetic order (LRO) even as $T \rightarrow 0$ K, despite strong magnetic interactions, and host fractionalized excitations such as spinons and Majorana fermions [6–10]. While QSLs are well understood in one-dimensional (1D) systems [11, 12], their realization in higher dimensions remains challenging. Following Anderson’s proposal of a QSL on the triangular lattice [13] and Kitaev’s model on the honeycomb lattice [14], numerous 2D QSL candidates have been identified [10, 15–20]. Interestingly, despite weaker quantum fluctuations in 3D, hyperkagome and pyrochlore lattices exhibit QSL-like signatures [21–24]. Identifying new 3D QSL materials could deepen our understanding of spin liquids and distinguish them from their 2D counterparts.

Notably, different types of spin liquids emerge depending

on spin-lattice symmetry [25]. One salient possibility is a chiral spin liquid (CSL), which, despite lacking LRO, breaks time-reversal and parity symmetries [26, 27]. The CSL state arises from chiral interactions like $\mathbf{S}_i \cdot (\mathbf{S}_j \times \mathbf{S}_k)$, involving spins at the vertices of a triangle [28]. Theoretically, the Heisenberg model with chiral interactions supports the CSL state in 2D frustrated lattices for $S = 1/2$ [28–31], while for $S \rightarrow \infty$, chiral interactions in 3D lattices could engender a classical CSL with fracton excitations [32]. The classical spin liquid state is characterized by an extensive ground-state degeneracy and can exhibit either algebraic or exponential spin correlations [33]. In 3D rare-earth pyrochlores, this brings about the emergence of a Coulomb phase with exotic monopole excitations and a U(1) gauge field [3, 34–37]. However, discovering suitable candidates to explore the classical CSL state is highly sought-after.

In this vein, newly discovered 3D trillium lattices provide a promising platform for delving into chiral phenomena, driven by their non-centrosymmetric chiral spin topology [38–46]. Trillium materials, such as MnSi and EuPtSi, which crystallize in the non-centrosymmetric space group $P2_13$, are found to host magnetic skyrmions [47] and chiral phonons [48]. Furthermore, trillium lattices, where classical spins form a 3D chiral network, have been proposed to manifest a spin ice-like classical spin liquid state, where a “two-in and one-out” configuration is satisfied on each triangle, contrasting with the “two-in and

* These authors contributed equally to this work.

† sankarndf@gmail.com

‡ choisky99@skku.edu

two-out” ice rules in pyrochlore lattices [49–51].

Herein, we report the ground-state properties of single-crystal $\text{K}_2\text{FeSn}(\text{PO}_4)_3$ (hereafter KFSPO), a $S = 5/2$ 3D trillium lattice compound, through thermodynamic, ESR, and μSR measurements. Magnetic susceptibility, specific heat, and ESR reveal a two-stage evolution of magnetic correlations across $T^* \approx 11$ K. Below T^* , dc and ac magnetic susceptibilities indicate weak magnetic ordering at $T_N \approx 2$ K under low fields, which is suppressed for $\mu_0 H \geq 2$ T, consistent with the weak field dependence of magnetic specific heat at low temperatures. μSR measurement confirms the dominance of persistent spin dynamics in both zero-field and 3.4 T, suggesting a dynamic spin-liquid-like ground state coexisting with quasistatic local fields.

II. EXPERIMENTAL DETAILS

High-quality single crystals of dipotassium iron(III) tin(IV) tris(orthophosphate), $\text{K}_2\text{FeSn}(\text{PO}_4)_3$, were successfully grown using a self-flux method within the pseudo-quaternary system $\text{K}_2\text{O}-\text{P}_2\text{O}_5-\text{Fe}_2\text{O}_3-\text{SnO}_2$. The stoichiometric amounts of SnO_2 (6.0 mmol), Fe_2O_3 (9.0 mmol), KPO_3 (5.62 mmol), and $\text{K}_4\text{P}_2\text{O}_7$ (3.1 mmol) were thoroughly ground and placed in a platinum crucible. The reactants were heated to 1150°C over 10 h and maintained at this temperature for 24 h. At this stage, the melt dissolved the metal oxides and was subsequently cooled to 750°C at a rate of 2°C per hour. After natural cooling to room temperature, pink-colored single crystals of KFSPO, predominantly tetrahedral in shape, were obtained from the remaining flux by leaching with deionized water [52].

Powder x-ray diffraction (XRD) measurements using a BrukerAXS (D8-Advance) x-ray diffractometer with Cu K_α radiation ($\lambda = 1.54$ Å) were performed on the crushed single crystals of KFSPO at room temperature. While the diffraction pattern for x-ray beam perpendicular to the (111) planes was obtained from high-resolution XRD (HR-XRD, Bruker AXS D8) with Cu K_α beam source. Detailed results of the XRD are presented in Supplementary Note 1 [53].

The dc magnetic susceptibility and magnetization measurements were performed using a superconducting quantum interference device vibrating sample magnetometer (SQUID-VSM, Quantum Design, USA) in the temperature range $2\text{ K} \leq T \leq 300\text{ K}$ and in magnetic fields up to 7 T. In addition, low-temperature dc magnetic susceptibility, magnetization, and ac magnetic susceptibility measurements were carried out down to 0.4 K using the ^3He option of the Quantum Design MPMS SQUID system.

High-field magnetization measurement was conducted at Dresden High Magnetic Field Laboratory, sweeping a magnetic field up to 55 T at 1.3 K using a nondestructive pulsed magnet along an arbitrary direction with respect to the crystal axes with the crystal orientation not

precisely determined. The obtained data were scaled to isothermal magnetization measurements obtained with a SQUID-VSM at the same temperature. Orientation-dependent magnetic susceptibilities are presented in Supplementary Note 2 [53].

Specific heat measurements were performed using a standard relaxation method with a physical property measurement system (PPMS, Quantum Design, USA) in the temperature range $2\text{ K} \leq T \leq 300\text{ K}$ and in magnetic fields up to 9 T. Furthermore, specific heat was measured in the temperature range $0.4\text{ K} \leq T \leq 4\text{ K}$ using ^3He option at Quantum Design Dynacool PPMS in several magnetic fields up to 9 T.

ESR measurements were performed using a conventional X-band ($f = 9.12\text{ GHz}$) ESR spectrometer (JEOL, JES-RE3X) in RIKEN. A single crystal of KFSPO was loaded on a quartz rod, applying the magnetic field along the [111] crystal orientation. A continuous ^4He -flow cryostat enabled controlling temperatures from 3.8 K to 280 K for the experiments.

Muon spin relaxation (μSR) experiments were conducted on the FLAME spectrometers at Paul Scherrer Institut (PSI) in Villigen, Switzerland under zero-field (ZF) and longitudinal field (LF) configurations. The initial muon spin direction was oriented along the beam direction. Many small crystals of KFSPO were mounted onto the sample holder using GE varnish and enclosed between two layers of $25\text{ }\mu\text{m}$ thick copper foil. A Variox system combined with a Kelvinox dilution fridge insert enabled measurements across a temperature range $30\text{ mK} \leq T \leq 100\text{ K}$ and a LF range of $0\text{ T} \leq \mu_0 H \leq 3.4\text{ T}$. The time evolution of the muon spin asymmetry at selected temperatures under an applied LF of $\mu_0 H = 3.4\text{ T}$ is shown in Supplementary Note 4 [53]. All the μSR spectra were modeled with a constant background $B_g \approx 0.013$, which remained nearly independent of both temperature and applied field. The μSR data were analyzed using the musrfit software [54]. Although high-quality single crystals of KFSPO were used, the enantiomeric purity of individual crystals was not verified. Since multiple crystals were measured simultaneously in the μSR experiments, it is likely that both enantiomers were present.

III. RESULTS

A. Crystal structure and x-ray diffraction

To confirm the phase purity of KFSPO, x-ray diffraction (XRD) measurements were performed on crushed single crystals. Rietveld refinement of the XRD (see Supplementary Note 1 [53] and Fig. 1) data reveals that the compound crystallizes in the cubic space group $P2_13$ with no detectable impurity phase [55]. The obtained atomic coordinates and lattice parameters are consistent with the previous report [52]. Fe^{3+} ions occupy two magnetic sites, each forming a trillium lattice, which is a chiral network of three equilateral triangular lattices (see Sup-

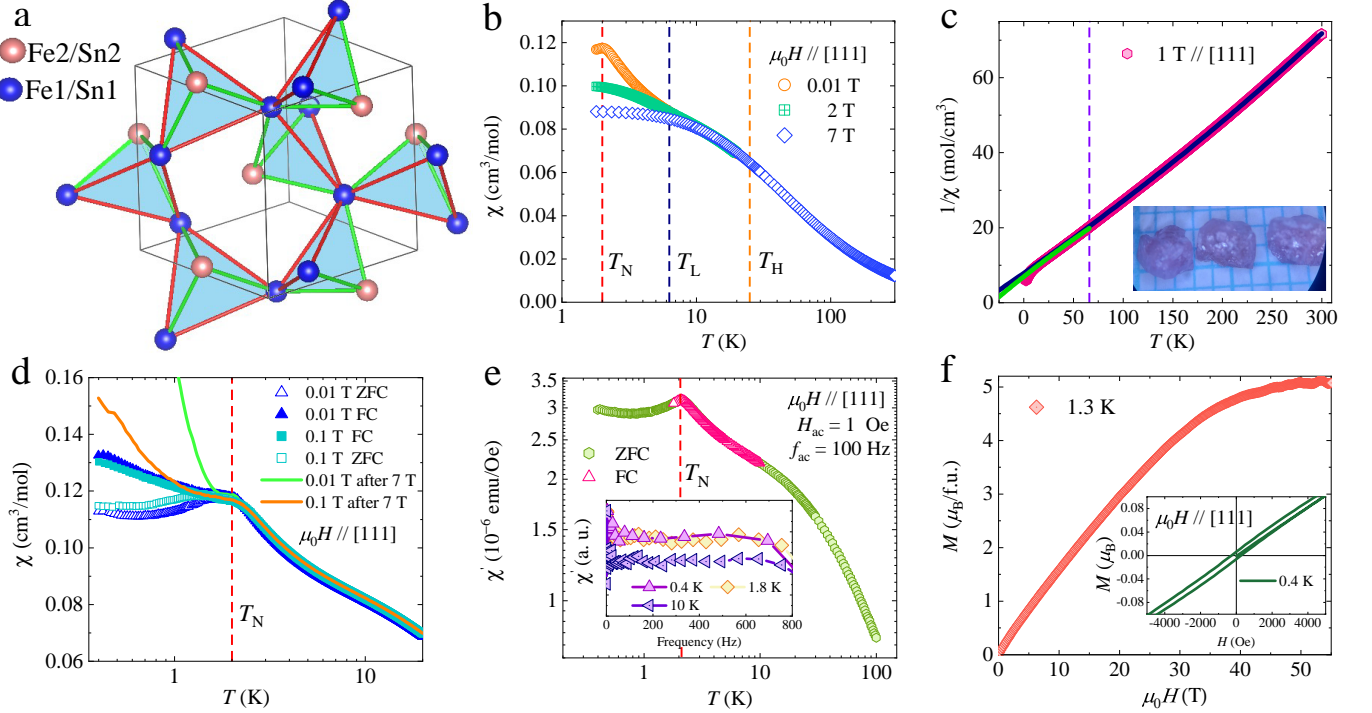


FIG. 1. (a) Featuring a hypertrillium lattice formed by two magnetic sites of Fe^{3+} ions, with a green bond length (Fe2–Fe1) of 4.96 Å and a red bond length (Fe1–Fe1) of 6.10 Å. (b) Temperature dependence of zero-field-cooled (ZFC) magnetic susceptibility at several magnetic fields applied parallel to the [111] direction. The dashed vertical lines around $T_L = 6.3$ K and $T_H = 25$ K indicate two characteristic features of magnetic correlations, and weak magnetic ordering at $T_N \approx 2$ K, as described in the text. (c) Temperature dependence of inverse magnetic susceptibility with a Curie-Weiss (CW) fit in two temperature regions, where deviation from the high-temperature CW fit is marked by a dashed vertical line around 66 K. Inset shows a photo of the single crystals. (d) Temperature dependence of ZFC and FC susceptibility at several fields in the temperature range $0.4 \text{ K} \leq T \leq 20 \text{ K}$. (e) Temperature dependence of real part of *ac* magnetic susceptibility (χ') at frequency $f_{ac} = 100$ Hz. Inset shows frequency dependence of normalized χ' at three different temperatures. (f) Isotherm magnetization as a function of magnetic field up to 55 T, with the field applied in an arbitrary orientation relative to the crystal axes. Inset shows the small hysteresis loop in magnetization isotherm at 0.4 K.

plementary [53] Fig. 1b). In the Fe1 trillium lattice, the exchange coupled Fe1-Fe2 bond length of 4.96 Å creates a 3D network of corner-sharing tetrahedra, known as the hypertrillium lattice, shown in Fig. 1(a). Like its sister compound $\text{K}_2\text{CrTi}(\text{PO}_4)_3$ [43], KFSPo exhibits unavoidable magnetic site dilution due to the similar atomic radii of Fe^{3+} (0.64 Å) and Sn^{4+} (0.62 Å) ions. Indeed, our XRD analysis confirms a significant degree of site dilution, with the Fe1 site 44(3)% occupied by Fe and 56(2)% by Sn, and the Fe2 site 55(3)% Fe and 45(1)% Sn (see Supplementary Note 1 [53]). Nevertheless, the remaining magnetic Fe ions are effectively interconnected through the Fe1–Fe2 network to sustain a 3D exchange topology. Even with partial Sn substitution, the Fe network maintains the connectivity of the hypertrillium lattice, enabling magnetic properties comparable to those seen in pristine magnetic Fe-based trillium systems [40]. As recently proposed [42], a key question is whether the dynamic spin correlations are intrinsically tied to the unique geometry of the hypertrillium lattice in the double trillium lattice systems. In this context, the observation of

a dynamic ground state despite substantial site dilution may point to the intrinsic robustness of the hypertrillium spin topology.

B. Magnetic susceptibility

Figure 1(b) shows the temperature dependence of zero-field-cooled (ZFC) *dc* magnetic susceptibility ($\chi(T)$) at several magnetic fields applied parallel to the [111] direction. Upon lowering the temperature, $\chi(T)$ exhibits a broad feature at $T_H = 25$ K (dashed orange line) with a subsequent increase below T_L . The broad feature indicates short-range spin correlations driven by thermal fluctuations in a system dominated by Heisenberg interactions [56]. On the other hand, the low-*T* increase is likely due to subdominant ferromagnetic interactions similar to that observed in the isostructural compound $\text{K}_2\text{CrTi}(\text{PO}_4)_3$ [43].

Upon further lowering temperature below T_L , $\chi(T)$ exhibits a weak kink at $T_N \approx 2$ K under $\mu_0 H = 0.01$ T, al-

luding to the occurrence of magnetic ordering. Moreover, for magnetic fields $\mu_0 H \geq 2$ T, the positions of T_L and T_H remain unchanged, while the weak kink around T_N is suppressed, triggering $\chi(T)$ to saturate at low temperatures (see [53]). This indicates that applying a magnetic field of $\mu_0 H \geq 2$ T quenches the weak ferromagnetic moments.

In order to estimate dominant exchange interactions between $S = 5/2$ spins of Fe^{3+} ions in KFSPo , the inverse magnetic susceptibility ($1/\chi(T)$) data were fitted by the Curie-Weiss (CW) law, $\chi(T) = \chi_0 + C/(T - \theta_{\text{CW}})$. Here, χ_0 is the sum of temperature-independent contributions of diamagnetic core susceptibility and Van-Vleck susceptibility, C is the Curie constant, and θ_{CW} represents the CW temperature. The high-temperature CW fit ($100 \text{ K} \leq T \leq 300 \text{ K}$, navy line in Fig. 1(c)) yields $\chi_0 = -2.56 \times 10^3 \text{ cm}^3/\text{mol}$, $C = 5.66(3) \text{ cm}^3 \text{ K}/\text{mol}$, and $\theta_{\text{CW}} = -43(2) \text{ K}$. The effective magnetic moment, $\mu_{\text{eff}} = \sqrt{8C} = 6.72(4) \mu_B$, is somewhat higher than the theoretical value of $\mu_{\text{eff}}^{\text{theo}} = 5.92 \mu_B$ for Fe^{3+} ($S = 5/2$), indicating the presence of moderate orbital contributions, similar to those observed in other trillium lattice compounds [45]. The obtained negative CW temperature suggests the presence of dominant antiferromagnetic interactions. Importantly, below 66 K, $\chi(T)$ deviates from the high-temperature Curie-Weiss fit and follows a secondary Curie-Weiss regime with $\theta_{\text{CW}} = -30 \text{ K}$, which is less negative than the high-temperature value ($\theta_{\text{CW}} = -43 \text{ K}$). This reduction suggests that subdominant ferromagnetic interactions become active at lower temperatures alongside dominant antiferromagnetic interactions (see below) [43].

To understand the nature of the weak kink around T_N , ZFC and FC susceptibility measurements were performed down to 0.4 K under two magnetic fields as shown in Fig. 1(d). The ZFC-FC bifurcation at $\mu_0 H = 0.01 \text{ T}$ implies the presence of ferromagnetic moments below T_N , while the reduced bifurcation at $\mu_0 H = 0.1 \text{ T}$ reflects the suppression of ferromagnetic moments with increasing field. Strikingly, field cycling to 7 T at 0.4 K alters $\chi(T)$ at 0.01 T (labeled as “after 7 T” in Fig. 1(d)), suggesting high-field-aligned ferromagnetic components retain partial alignment after reducing the field, yielding distinct magnetic responses. The absence of frequency dependence in the ac magnetic susceptibility (inset of Fig. 1(e)) above and below T_N rules out conventional spin freezing, confirming that the irreversibility in $\chi(T)$ arises from a weak ferromagnetic moment [43]. Even though our ac magnetic susceptibility measurements are limited to low frequencies, the absence of conventional spin freezing or spin glass is further supported by our μSR experiments (see sec. III E) [57]. This also indicates that magnetic site dilution in the three-dimensionally connected, double trillium lattices gives rise to novel 3D frustrated spin networks, without introducing exchange randomness or quenched disorder. Additionally, the weak kink in the real part of ac magnetic susceptibility (Fig. 1(e)) further supports the presence of weak magnetic ordering in the

title compound.

To further confirm the presence of subdominant ferromagnetic interactions, isotherm magnetization measurements were performed at several temperatures as shown in Supplementary Fig. 2(b). At 0.4 K, a weak but distinct hysteresis at low fields supports the presence of weak ferromagnetic moment below T_N (inset of Fig. 1(f)). Above 6 K, however, the linear response indicates dominant antiferromagnetic interactions. Before proceeding, we note that the presence of subdominant ferromagnetic interactions, the observed ZFC/FC splitting, and the absence of frequency dependence in the ac susceptibility collectively suggest that the non-centrosymmetric chiral crystal structure may give rise to moment canting via Dzyaloshinskii-Moriya interactions (DMIs). This, in turn, could lead to weak canted antiferromagnetic ordering below T_N [43, 58]. To determine precisely the nature of the magnetic ordering, further neutron diffraction studies are required.

Pulsed-field magnetization measurements up to 55 T show saturation at $5 \mu_B$ above 43 T, with no sign of a $1/3$ magnetization plateau unlike the classical spin-liquid candidate $\text{Na}[\text{Mn}(\text{HCOO})_3]$ ($S = 5/2$) with a single trillium lattice [51]. This absence implies that the hypertrillium lattice involves additional interactions beyond the Heisenberg model.

C. Magnetic specific heat

To gain deeper insights into the magnetic behavior, specific heat measurements were conducted under various magnetic fields. Figure 2(a) shows the temperature dependence of magnetic specific heat, C_{mag} , obtained after subtracting lattice contributions at several magnetic fields (see Supplementary Note 3 [53]) [59, 60]. C_{mag} begins to increase below 70 K, suggesting the growth magnetic correlations well above θ_{CW} . A broad peak around $T_H = 25 \text{ K}$ signifies that these correlations evolve toward saturation, consistent with the $\chi(T)$ data (Fig. 1(b)). In classical spin systems with competing interactions, the spin configuration remains degenerate at finite temperatures, fluctuating among multiple low-energy states before stabilizing at lower temperatures due to subleading terms [56]. This high-temperature regime, often termed as a classical paramagnetic region, spans from T_H to $\sim 66 \text{ K}$ in our system. Notably, the pronounced anomaly around $T_L = 6.3 \text{ K}$ alludes to the formation of a well-structured spin configuration, potentially driven by subdominant ferromagnetic interactions [32]. Temperature dependence of entropy change is shown in Fig. 2(b) at zero-field. The power-law behavior (see below) is extrapolated to zero temperature to compute a total magnetic entropy. At T_L , the magnetic entropy is $0.45 R \ln(6)$, reflecting partial entropy release, typical of classical systems with a degenerate ground state. The entropy reaches its full theoretical value, $R \ln(6)$, above θ_{CW} . The absence of any anomaly in

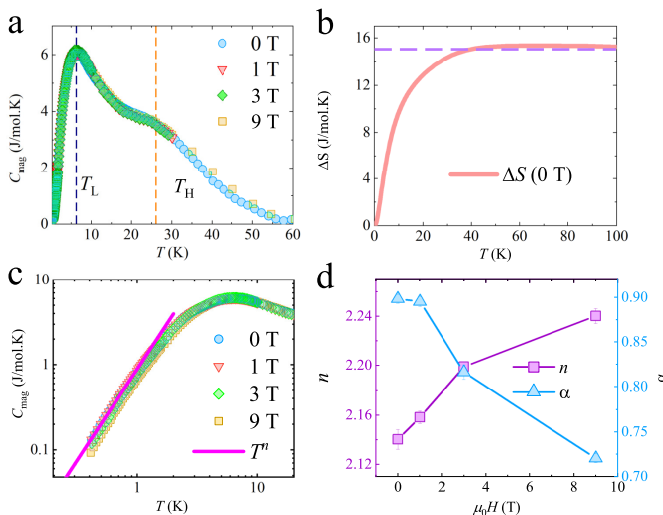


FIG. 2. (a) Temperature dependence of magnetic specific heat (C_{mag}) at several magnetic fields. The vertical dashed line represents two characteristic temperatures around $T_L = 6.3$ K and $T_H = 25$ K. (b) Temperature dependence of entropy change at zero-field. The dashed horizontal line indicates the expected entropy, $R \ln(2S + 1)$, for $S = 5/2$. (c) C_{mag} as a function of temperature where the solid red line showing the power-law behavior ($\approx \alpha T^n$). (d) Field dependence of exponent (n) and the coefficient (α). Error bars represent an uncertainty of one standard deviation.

C_{mag} from weak magnetic ordering around T_N , observed in $\chi(T)$, highlights its subtle nature. Furthermore, the field-dependent suppression of the weak kink in $\chi(T)$ is reflected in the low-temperature behavior of C_{mag} below 3 K.

At $T \ll T_N$, C_{mag} shows a power-law dependence, $C_{\text{mag}} = \alpha T^n$, indicating the presence of gapless excitations, as shown in Fig. 2(c). The obtained exponent n and coefficient α are plotted as functions of the applied magnetic field in Fig. 2(d). Interestingly, the exponent increases from 2.13(1) to 2.24(1) with increasing magnetic field up to 9 T. The associated density of excitations, represented by α , is suppressed with increasing field. Notably, the nearly quadratic temperature dependence of C_{mag} has been observed in other 3D systems [38, 40, 61] and is considered evidence for non-trivial, gapless excitations. More importantly, this quadratic behavior is also found in $\text{KSrFe}_2(\text{PO}_4)_3$ [40], an isostructural compound without site mixing, indicating that Fe/Sn site disorder has minimal impact on magnetic behavior. If such disorder were significant, a random-singlet state would be stabilized, resulting in $C_{\text{mag}}/T \propto T^{-n}$ with $n < 1$ [62]

D. Electron spin resonance

To trace a thermal evolution of spin correlations, X-band ESR measurements were performed down to 3.8

K at $f = 9.12$ GHz for $\mu_0 H \parallel [111]$ (Fig. 3(a)). An exchange-narrowed single resonance line is observed across all temperatures, fitted with a derivative Lorentzian function. As the temperature decreases, the ESR signal broadens all the way down to 3.8 K. A signal from an experimental artifact is marked by a triangle at the lowest temperature. The extracted ESR parameters, including integrated intensity, g -factor, and linewidth, as a function of temperature, are shown in Fig. 3(b) and Fig. 3(c). The integrated intensity follows $\chi(T)$ down to 65 K (green dashed line in Fig. 3(b)), after which it deviates and increases sharply. Below 7 K, the intensity abruptly decreases. This deviation coincides with the low- T departure from the high- T CW fit, suggesting a change in spin correlations around 65 K.

The buildup of the internal field is reflected in the g -value shift (inset of Fig. 3(c)). Above 140 K, the g -value is 2.010(3), close to the expected 2.002(3) for half-filled Fe^{3+} ($S = 5/2$), and increases gradually as the temperature decreases. At 3.8 K, the g -value rises sharply to 2.16, indicating the development of critical-like spin fluctuations towards 3.8 K.

The temperature-dependent evolution of spin correlations is more evident in the linewidth broadening (Fig. 3(c)). The ESR linewidth increases across the entire temperature range, even up to 280 K. This persistence of linewidth broadening up to $\sim 7\theta_{\text{CW}}$ is typical for low-dimensional frustrated magnets but unusual for 3D frustrated lattices.

To further analyze this, the ESR linewidth is fitted with a power-law function, $\mu_0 \Delta H \propto T^{-p}$. The fitting reveals two distinct regimes: $p = 1.12 \pm 0.01$ down to 10 K and $p = 1.5 \pm 0.3$ below 10 K. These different exponents indicate a change in spin correlations at the crossover temperature $T^* = 11$ K. As discussed, the spin correlations between T^* and $T = 298$ K are attributed to dominant antiferromagnetic Heisenberg interactions, while below T^* , a subleading term stabilizes a well-defined correlated spin configuration, accompanied by a slowdown of spin fluctuations [63]. We note that two-stage linewidth broadening is also observed in other frustrated magnets, including the trillium lattice compound $\text{K}_2\text{CrTi}(\text{PO}_4)_3$ [43, 63–65].

E. Muon spin relaxation

To gain additional insight into spin dynamics in KF-SPO , ZF and LF μSR measurements were performed over wide temperature and field ranges. The implanted 100% spin-polarized muons localize at an interstitial lattice site, typically 1 Å from oxygen ions in KF-SPO [66].

In the polycrystalline samples with long-range magnetic order, the muon spin polarization typically exhibits coherent oscillations corresponding to the 2/3 transverse component and a non-oscillating 1/3 longitudinal component. As shown in Fig. 4(a), the time evolution of the muon spin polarization down to $T = 30$ mK reveals

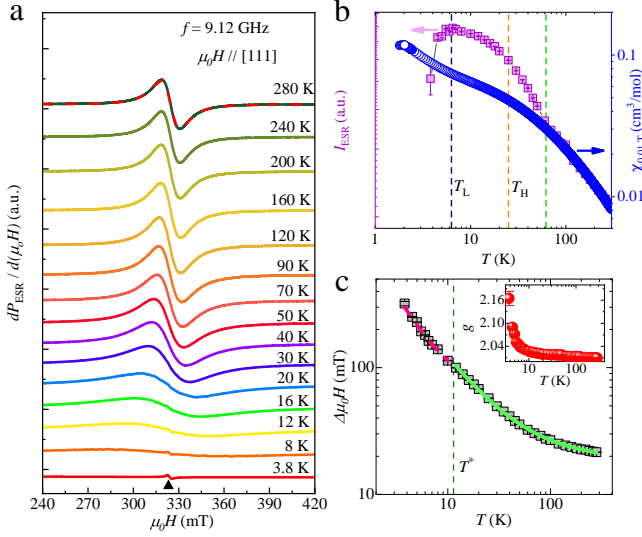


FIG. 3. (a) Representative ESR spectra at $f = 9.12$ GHz at various temperatures with the magnetic field applied to [111] crystal orientation. All spectra are offset for clarity. The dashed red line on the spectrum at $T = 280$ K represents the fitting using a derivative Lorentzian function. (b) Temperature dependence of the integrated ESR intensity (left-y axis). The blue data points in right-y axis represent the $\chi(T)$ data at $\mu_0 H = 0.01$ T from Fig. 1(b). The positions of the dashed vertical lines are detailed in the text. (c) Temperature dependence of the peak-to-peak linewidth, and the g -factor (in the inset) obtained from the fittings of the ESR spectra shown in (a). The red dashed and solid green curves in linewidth represent the fit of the data using a power-law function (see the text in detail). The dashed vertical line at $T^* \approx 11$ K indicates the crossover between two power-law behaviors. (b) and (c) are log-log plots. Error bars represent an uncertainty of one standard deviation.

neither coherent oscillations indicative of static magnetic order, nor the typical “1/3” tail associated with the randomly oriented static internal fields (spin-freezing) in KFSPO [67]. On the other hand, in the fast fluctuation limit—where all three spatial components become equivalent—one would expect the absence of the characteristic “1/3” tail. In KFSPO, as the temperature decreases below T_L , the polarization shows a gradual development of rapid decay at early times ($t \ll 0.2 \mu\text{s}$), (Fig. 4(b)) indicating muon senses a static distribution of internal magnetic fields over the muon lifetime, while the remaining relaxation persisting to late times suggests the presence of fluctuating electronic moments. This scenario implies that KFSPO resides in an intermediate regime between the static and fast fluctuation limits, consistent with the presence of weak magnetic order. Furthermore, as discussed in the following section, the observed muon spin polarization differs from that often seen in 3D spin-liquid candidates where static moments from spin freezing coexist with dynamic moments [57, 68]. For a quantitative analysis, various models were tested,

and the function $P(t)_{\text{ZF}} = \exp[-\lambda_{\text{ZF}} t] + Bg$ (solid line in Fig. 4(a)) was found to best describe the ZF spectra down to T_L , where Bg represents a constant background from muons stopping outside the sample. This Lorentzian form of muon spin polarization captures the cooperative dynamics of fluctuating local electronic moments, which give rise to the muon spin relaxation rate λ_{ZF} . However, for $T < T_L$, the ZF spectra down to 30 mK require the polarization function (solid line in Fig. 4(a)) $P(t)_{\text{ZF}} = f_{\text{ZF}} \exp[-\lambda_{\text{ZF}} t] + (1 - f_{\text{ZF}}) \exp[-\frac{1}{2}(\sigma_{\text{ZF}} t)^2] + Bg$, where the second term, which dominates at early times and reflects a Gaussian distribution of quasistatic internal fields at the muon site, becomes necessary to account for the low-temperature behavior of the polarization (see Fig. 4(b)). Here, f_{ZF} and $(1 - f_{\text{ZF}})$ represent the fractions of dynamic and quasistatic components of the signal, respectively, while σ_{ZF} corresponds to the muon spin relaxation rate associated to the fast relaxing static component.

The temperature dependence of obtained λ_{ZF} is shown in Fig. 4(c) in ZF. For $T > T^* = 11$ K, λ_{ZF} remains constant originating from the exchange fluctuations of electronic spins of Fe^{3+} ions in the motional narrowing regime. Using the mean-field approximation for average exchange interaction $J = 3k_B\theta_{\text{CW}}/2zS(S+1)$ with the nearest-neighbor coordination number $z = 6$ and $S = 5/2$, the exchange fluctuation rate is estimated as $\nu = \sqrt{z}JS/\hbar = 9.78 \times 10^{11} \text{ s}^{-1}$ [69]. This gives the internal field distribution width $\Delta/\gamma_\mu = \sqrt{\nu\lambda_{\text{ZF}}/2}/\gamma_\mu \approx 3 \text{ kG}$ at high temperatures, where $\lambda_{\text{ZF}} = 0.165 \mu\text{s}^{-1}$ ($T \gg T^*$) and the muon gyromagnetic ratio $\gamma_\mu = 2\pi \times 135.5 \text{ MHz/T}$. As the temperature decreases below T^* , λ_{ZF} increases by nearly a factor of six, attributed to the slowing down of spin fluctuations. Furthermore, the T -independent plateau behavior observed at low temperatures indicates the presence of persistent spin dynamics, a common characteristic of spin liquid candidates. Persistent spin dynamics accommodated by the two components of the muon spin relaxation rate, are also observed in other trillium lattice systems despite undergoing symmetry-breaking phase transitions [38, 43].

The extracted Gaussian relaxation rate, which originates from quasistatic local moments, is shown in Fig. 4(d) as a function of temperature. It exhibits a sudden increase by several orders of magnitude with a slight temperature rise below T_L , followed by a tendency toward saturation below 1 K. The temperature independence of σ_{ZF} below 1 K suggests that the system enters a quasistatic regime characterized by slow spin dynamics. The temperature dependence of f_{ZF} and $(1 - f_{\text{ZF}})$, shown in Supplementary Fig. 4(a), reflects the fractions of dynamic and static components, respectively. Notably, both components remain nearly temperature-independent below 1 K with $\approx 80\%$ quasistatic and $\approx 18\%$ dynamic signal fractions, indicating the coexistence of quasistatic and fluctuating local electronic moments in the ground state. However, a distinct increase of f_{ZF} accompanied by a corresponding decrease of f_{ZF} is observed down to

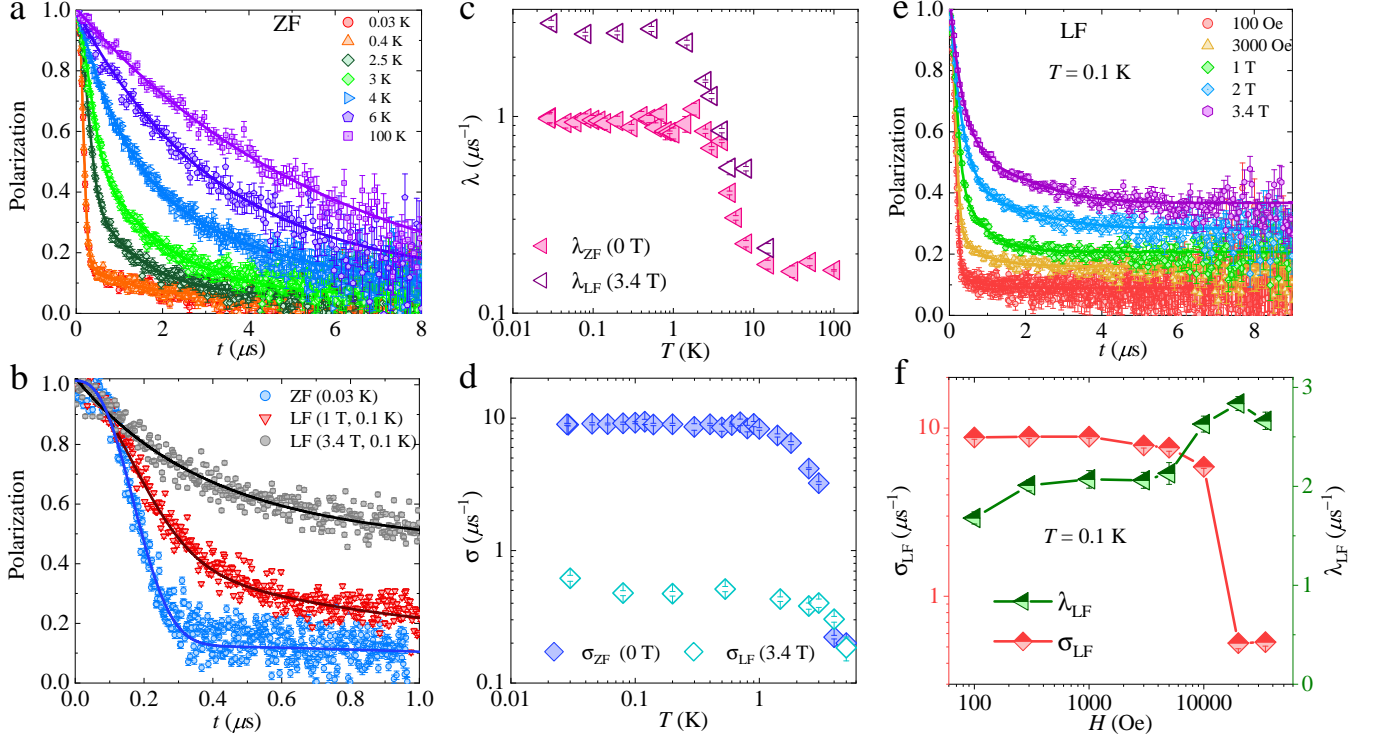


FIG. 4. (a) Time evolution of normalized muon spin polarization in ZF for a few representative temperatures over a long-time scale. (b) Time evolution of normalized muon spin polarization in ZF at $T = 0.03$ K and under two LFs at $T = 0.1$ K at short times. (c) Temperature dependence of the exponential muon spin relaxation rates at late times in ZF and LF of $\mu_0 H = 3.4$ T. (d) Temperature dependence of the Gaussian relaxation rates at early times in ZF and LF of $\mu_0 H = 3.4$ T. (e) Field dependence of the normalized muon spin polarization at $T = 0.1$ K. (f) Gaussian (left y -axis) and exponential (right y -axis) muon spin relaxation rate as a function of LF at 0.1 K. Error bars represent an uncertainty of one standard deviation.

T_L . Above T_L , the dynamic fraction persists to higher temperatures and closely tracks the crossover temperature T^* . It is worth noting that at low temperatures the $\sim 18\%$ exponential relaxation component is primarily attributed to weakly ordered moments that remain dynamic. The remaining $\sim 80\%$, exhibiting anomalous Gaussian-like muon spin polarization, likely reflects characteristics common to classical spin-liquid-like systems, as observed in $\text{SrCr}_8\text{Ga}_4\text{O}_{19}$ [69]. In the trillium lattice $\text{K}_2\text{Ni}_2(\text{SO}_4)_3$, a similar exponential component has been attributed to partial homogeneous ordering [38], while the remaining relaxation arises from sporadic unpaired-spin excitations, consistent with our observation of an undecoupled Gaussian relaxation in both ZF and LF data (discussed below). Compared to the $S = 1$ trillium lattice system $\text{K}_2\text{Ni}_2(\text{SO}_4)_3$ [38], our $S = 5/2$ system exhibits more classical spin behavior, characterized by a stronger growth of the static fraction below T_L , likely due to sporadic unpaired-spin excitations, as suggested by the decoupling experiments described below [38, 43, 69]. In order to find the intrinsic origin of Gaussian distribution of local internal fields at low temperatures, μSR measurements were conducted at $T = 0.1$ K under several LFs which decouples the polarization from purely static

and random local fields. As shown in Fig. 4(e), even when applying LFs exceeding the expected local field from ZF data ($\Delta/\gamma_\mu \approx 3$ kG), the decoupling of the muon spin polarization remains minimal. This weakness of the field dependence of polarization suggests that the Gaussian distribution of local fields manifests a distinct fingerprint in the present correlated system. Furthermore, if the Gaussian distribution of local fields were static at low temperatures, full polarization would be recovered in a LF of 3.4 T (Fig. 4(e)). The strong residual “undecouplable Gaussian” line shape at early times can be attributed to the presence spin excitations (e.g., spinons) which contribute to Gaussian shape muon relaxation on the background of a quasistatic frozen state [69]. A similar behavior has been observed in other spin liquid candidates including the double trillium lattice compound $\text{K}_2\text{Ni}_2(\text{SO}_4)_3$ [38] and the kagome lattice $\text{SrCr}_8\text{Ga}_4\text{O}_{19}$ [69].

To further confirm the robustness of the spin liquid signature even under a high magnetic field, μSR measurements were conducted at a LF of 3.4 T in the T -range $30 \text{ mK} \leq T \leq 15 \text{ K}$ (see Supplementary Fig. 4(b)). The μSR data in LF were modeled using the function $P(t)_{\text{LF}} = f_{\text{LF}} \exp[-\lambda_{\text{LF}} t] + (1 - f_{\text{LF}}) \exp[-\frac{1}{2}(\sigma_{\text{LF}} t)^2] +$

B_g . The parameter $f_{LF}(1-f_{LF})$ corresponds to the fraction of the dynamic(quasistatic)-relaxing component. Its value remains nearly temperature-independent below T_L , with approximately 80% dynamic and 20% static contributions (see Supplementary Fig. 4(c)). The obtained λ_{LF} and σ_{LF} relaxation rates in a LF of $\mu_0 H = 3.4$ T are compared with those obtained from the ZF data in Fig. 4(c) and Fig. 4(d). The temperature dependence of both relaxation rates at 3.4 T reveals the presence of persistent spin dynamics within a weak quasistatic regime.

Interestingly, in a LF of 3.4 T particularly below T_L , the quasistatic component decreases by 75% compared to ZF, and the corresponding relaxation rate drops sharply by 93 %, indicating the suppression of low-energy spin excitations that govern the muon spin relaxation. This is further corroborated by the field dependence of the parameter α (Fig. 2(d)), which reflects the density of such excitations. On the other hand, the dynamic component increases nearly fivefold, and its relaxation rate rises by almost three orders of magnitude, suggesting the decoupling of static local fields—consistent with the field-induced suppression of weak magnetic order and field-resilient spin dynamics, as evidenced by the enhanced Lorentzian fraction and rate.

Figure 4(f) shows the LF dependence of σ_{LF} (left y -axis) and λ_{LF} (right x -axis), highlighting the suppression of low-energy excitations—evident from the reduced Gaussian relaxation rate and enhanced dynamic relaxation rate due to the decoupling of quasistatic fields. This scenario can be correlated with the field dependence of the coefficient α and the power-law exponent n in the magnetic specific heat expression, $C_{mag} \approx \alpha T^n$ at low temperatures.

IV. DISCUSSION

We first address the weak magnetic ordering at $T_N \approx 2$ K, seen from subtle kinks in both dc and ac magnetic susceptibility. We recall that the non-centrosymmetric chiral cubic space group $P2_13$ lacks inversion symmetry but permits DMIs, which can induce weak ferromagnetism [58]. For example, in the trillium lattice compound $Cs_2Fe_2(MoO_4)_3$ ($T_N \approx 1$ K), DMIs are thought to contribute to the presence of subdominant ferromagnetic exchange [45]. Similarly, trillium lattices in $P2_13$ often host ferromagnetic interactions in addition to dominant antiferromagnetic ones [43, 70]. Given that KFSPO shares this symmetry, weak ferromagnetism driven by DMIs is expected, consistent with the canted antiferromagnetic order seen in the related compound $K_2CrTi(PO_4)_3$ [43]. However, unlike magnetic susceptibility, magnetic specific heat and μ SR do not clearly detect this ordering, highlighting its subtlety. Such hidden order is often reported in trillium compounds; for instance, $K_2CrTi(PO_4)_3$ shows no ordering in susceptibility but clear signatures in specific heat [43], while in $K_2Ni_2(SO_4)_3$, specific heat reveals ordering that

μ SR does not clearly capture [38].

Despite the presence of weak magnetic order, it is observed that strong spin fluctuations, which may arise from the hypertrillium spin topology, can lead to persistent spin dynamics without a clear signature of magnetic ordering as observed in μ SR experiments for $K_2Ni_2(SO_4)_3$ [38]. A similar scenario is expected in the titled compound KFSPO, where weak magnetic ordering may lead to a fraction quasistatic fast relaxation superimposed on a dominant uncoupled Gaussian relaxation associated with non-trivial spin excitations, along with additional relaxation from persistent spin dynamics. This Gaussian like relaxation from low-energy excitations is also observed in $K_2Ni_2(SO_4)_3$, indicating a common feature of the hypertrillium spin topology that is maintained despite anti-site disorder in KFSPO. Most importantly, if the Gaussian relaxation originates entirely from disorder-induced quasistatic moments, this should be reflected in our decoupling experiments as a saturation of the full polarization at fields $3.4\text{ T} > \Delta/\gamma_\mu$. Therefore, the absence of full recovery of muon spin polarization in LF- μ SR experiments provides concrete evidence for disorder-induced smearing of the LRO state in KFSPO. An alternative scenario of disorder-induced quasistatic magnetic field is often identified through Gaussian-broadened relaxation of the muon spin polarization function, as observed in α - $Ru_xIr_{1-x}Cl_3$ [71] and $K_2CrTi(PO_4)_3$ [43]. The anomalous LF dependence of the muon spin polarization in KFSPO may suggest the presence of classical spin-liquid-like correlations, similar to that observed in the $S = 3/2$ $SrCr_8Ga_4O_{19}$ system [69].

A close comparison between the two isostructural $S = 5/2$ trillium compounds, KFSPO and $KSrFe_2(PO_4)_3$ [40]—where KFSPO exhibits magnetic site dilution (Fe/Sn) and $KSrFe_2(PO_4)_3$ displays non-magnetic site disorder (Sr/K)—reveals that the key difference lies in the temperature at which the ZFC/FC splitting occurs. In contrast, the specific heat behavior is remarkably similar in both systems. This suggests that magnetic site dilution primarily affects the weak ferromagnetic interactions while preserving the essential spin dynamics associated with the trillium lattice topology. Nevertheless, given the substantial magnetic site randomness in KFSPO, a natural question arises regarding the possibility of a random-singlet state [72–74], similar to those proposed in other disordered frustrated magnets, such as the $S = 1/2$ systems $Sr_2CuTe_{1-x}W_xO_6$ [73] and Li_4CuTeO_6 [62], and the $S = 5/2$ system $Lu_3Sb_3Mn_2O_{14}$ [75].

Experimental signatures of the random singlet state manifest as power-law behaviors in physical observables such as magnetic susceptibility ($\chi \propto T^{-\alpha}$), specific heat ($C_{mag}/T \propto T^{-\alpha}$), ESR linewidth ($\Delta H \propto T^{-\alpha}$), and muon spin relaxation rate ($\lambda_{ZF} \propto T^{-\alpha}$) [62, 73, 75]. The exponent α ($0 < \alpha < 1$) reflects the probability distribution of random exchange interactions, described by $P(J) \propto J^{-\alpha}$. The absence of a similar power-law

dependence in KFSPO indicates that its ground state deviates from the random singlet state. The absence of a characteristic power-law dependence and its scaling in KFSPO suggests that its ground state deviates from a random-singlet scenario. There is no direct calculation for the percolation threshold of a trillium lattice. Given a 3D network with a coordination number of 4, the site percolation threshold for the trillium lattice is likely close to 0.43, similar to the diamond lattice (coordination 4) [76]. The lack of random-singlet phenomenology may be attributed to the relatively low percolation threshold of the trillium lattice, estimated to be $p_c \sim 0.43$ [76]. It is highly likely that the Fe occupancy on the two interpenetrating trillium sublattices exceeds this threshold, thereby preserving long-range magnetic connectivity despite Fe/Sn site disorder. Notably, KFSPO shows closer resemblance to the spin dynamics observed in the $S = 3/2$ system $\text{SrCr}_8\text{Ga}_4\text{O}_{19}$ [61, 69, 77], and exhibits short-range spin correlations above T_N , similar to those reported in the $S = 5/2$ classical spin liquid candidate $\text{Li}_9\text{Fe}_3(\text{P}_2\text{O}_7)_3(\text{PO}_4)_2$ [78]. Although the title compound displays experimental features characteristic of classical spin liquid behavior [33], subleading interactions and disorder appear to stabilize weak magnetic ordering and introduce inhomogeneity in the spin dynamics and the ground state.

V. CONCLUSION

In summary, through a combination of bulk and local probe experiments, we investigate the ground-state properties of a 3D trillium lattice compound $\text{K}_2\text{FeSn}(\text{PO}_4)_3$, where Fe^{3+} ions form a chiral network of corner-sharing tetrahedra, known as a hypertrillium lattice. The two-step evolution of magnetic correlations, as revealed by ESR linewidth, coupled with two distinct anomalies in specific heat separated by $T^* \approx 11$ K, points to a complex interplay between dominant antiferromagnetic Heisenberg interactions and subleading interaction terms in this system. Furthermore, the weak magnetic

ordering at $T_N \approx 2$ K is revealed only through *dc* and *ac* magnetic susceptibility measurements, suggesting its subtle nature. This weak ordering is suppressed under an applied field $\mu_0 H \geq 2$ T, corroborated by the weak field dependence of the magnetic specific heat. Despite the symmetry-breaking transition, μSR results reveal dominant persistent spin dynamics, suggesting a spin-liquid-like ground state coexisting with weak magnetic order. Our experimental results underscore the importance of further studies, particularly using inelastic neutron scattering, to clarify the nature of the subleading interactions.

VI. DATA AVAILABILITY

The μSR data that support the findings of this paper are openly available [79]. All other data, including magnetic susceptibility, magnetization, specific heat, and ESR, are available upon reasonable request.

VII. ACKNOWLEDGMENTS

The work at SKKU was supported by the National Research Foundation (NRF) of Korea (Grants No. RS-2023-00209121 and No. 2020R1A5A1016518). E.M. is supported by the Canada Research Chairs program, the Natural Science and Engineering Research Council of Canada, and the Canadian Foundation for Innovation. This work was supported by HLD-HZDR, member of the European Magnetic Field Laboratory (EMFL). R. S. acknowledges the financial support provided by the Ministry of Science and Technology in Taiwan under Project No. NSTC-113-2124-M-001-003 and No. NSTC-113-2112M001-045-MY3, as well as support from Academia Sinica for the budget of AS-iMATE11312. financial support from the Center of Atomic Initiative for New Materials (AIMat), National Taiwan University, under Project No. 113L900801. This work is partially based on experiments performed at the Swiss Muon Source μS , Paul Scherrer Institute, Villigen, Switzerland.

-
- [1] L. Balents, Spin liquids in frustrated magnets, *Nature* **464**, 199 (2010).
 - [2] L. Savary and L. Balents, Quantum spin liquids: a review, *Rep. Prog. Phys.* **80**, 016502 (2016).
 - [3] C. L. Henley, The “coulomb phase” in frustrated systems, *Annu. Rev. Condens. Matter Phys.* **1**, 179 (2010).
 - [4] G. C. Lau, R. S. Freitas, B. G. Ueland, B. D. Muegge, E. L. Duncan, P. Schiffer, and R. J. Cava, Zero-point entropy in stuffed spin-ice, *Nat. Phys.* **2**, 249 (2006).
 - [5] Z. Bacciconi, H. Xavier, I. Carusotto, T. Chanda, and M. Dalmonte, *Theory of fractional quantum Hall liquids coupled to quantum light and emergent graviton-polaritons* (2024), [arXiv:2405.12292 \[cond-mat.mes-hall\]](https://arxiv.org/abs/2405.12292).
 - [6] J. Khatua, B. Sana, A. Zorko, M. Gomilšek, K. Sethupathi, M. R. Rao, M. Baenitz, B. Schmidt, and P. Khuntia, Experimental signatures of quantum and topological states in frustrated magnetism, *Phys. Rep.* **1041**, 1 (2023).
 - [7] H. Takagi, T. Takayama, G. Jackeli, G. Khaliullin, and S. E. Nagler, Concept and realization of Kitaev quantum spin liquids, *Nat. Rev. Phys.* **1**, 264 (2019).
 - [8] C. Broholm, R. J. Cava, S. A. Kivelson, D. G. Nocera, M. R. Norman, and T. Senthil, Quantum spin liquids, *Science* **367**, eaay0668 (2020).
 - [9] J. Nasu, Majorana quasiparticles emergent in Kitaev spin liquid, *Prog. Theor. Exp. Phys.*, ptad115 (2023).

- [10] J. A. Sears, L. E. Chern, S. Kim, P. J. Bereciartua, S. Francoual, Y. B. Kim, and Y.-J. Kim, Ferromagnetic Kitaev interaction and the origin of large magnetic anisotropy in α -RuCl₃, *Nat. Phys.* **16**, 837 (2020).
- [11] D. A. Tennant, R. A. Cowley, S. E. Nagler, and A. M. Tsvetlik, Measurement of the spin-excitation continuum in one-dimensional KCuF₃ using neutron scattering, *Phys. Rev. B* **52**, 13368 (1995).
- [12] B. Lake, D. A. Tennant, J.-S. Caux, T. Barthel, U. Schollwöck, S. E. Nagler, and C. D. Frost, Multispinon continua at zero and finite temperature in a near-ideal Heisenberg chain, *Phys. Rev. Lett.* **111**, 137205 (2013).
- [13] P. W. Anderson, Resonating valence bonds: A new kind of insulator?, *Mater. Res. Bull.* **8**, 153 (1973).
- [14] A. Kitaev, Anyons in an exactly solved model and beyond, *Ann. Phys.* **321**, 2–111 (2006).
- [15] S. Jeon, D. Wulferding, Y. Choi, S. Lee, K. Nam, K. H. Kim, M. Lee, T.-H. Jang, J.-H. Park, S. Lee, S. Choi, C. Lee, H. Nojiri, and K.-Y. Choi, One-ninth magnetization plateau stabilized by spin entanglement in a kagome antiferromagnet, *Nat. Phys.* **20**, 435 (2024).
- [16] P. Khuntia, M. Velazquez, Q. Barthélemy, F. Bert, E. Kermarrec, A. Legros, B. Bernu, L. Messio, A. Zorko, and P. Mendels, Gapless ground state in the archetypal quantum kagome antiferromagnet ZnCu₃(OH)₆Cl₂, *Nat. Phys.* **16**, 469 (2020).
- [17] R. Bag, S. Xu, N. E. Sherman, L. Yadav, A. I. Kolesnikov, A. A. Podlesnyak, E. S. Choi, I. da Silva, J. E. Moore, and S. Haravifard, Evidence of dirac quantum spin liquid in YbZn₂GaO₅, *Phys. Rev. Lett.* **133**, 266703 (2024).
- [18] Y. Li, YbMgGaO₄: A triangular-lattice quantum spin liquid candidate, *Adv. Quantum Technol.* **2**, 1900089 (2019).
- [19] T. Arh, B. Sana, M. Pregelj, P. Khuntia, Z. Jagličić, M. D. Le, P. K. Biswas, P. Manuel, L. Mangin-Thro, A. Ozarowski, and A. Zorko, The Ising triangular-lattice antiferromagnet neodymium heptatantalate as a quantum spin liquid candidate, *Nat. Mater.* **21**, 416 (2022).
- [20] M. M. Bordelon, E. Kenney, C. Liu, T. Hogan, L. Posthuma, M. Kavand, Y. Lyu, M. Sherwin, N. P. Butch, C. Brown, M. J. Graf, L. Balents, and S. D. Wilson, Field-tunable quantum disordered ground state in the triangular-lattice antiferromagnet NaYbO₂, *Nat. Phys.* **15**, 1058 (2019).
- [21] S. Chillal, Y. Iqbal, H. O. Jeschke, J. A. Rodriguez-Rivera, R. Bewley, P. Manuel, D. Khalyavin, P. Steffens, R. Thomale, A. T. M. N. Islam, J. Reuther, and B. Lake, Evidence for a three-dimensional quantum spin liquid in PbCuTe₂O₆, *Nat. Commun.* **11**, 2348 (2020).
- [22] P. Khuntia, F. Bert, P. Mendels, B. Koteswararao, A. V. Mahajan, M. Baenitz, F. C. Chou, C. Baines, A. Amato, and Y. Furukawa, Spin liquid state in the 3D frustrated antiferromagnet PbCuTe₂O₆: NMR and Muon spin relaxation studies, *Phys. Rev. Lett.* **116**, 107203 (2016).
- [23] K. W. Plumb, H. J. Changlani, A. Scheie, S. Zhang, J. W. Krizan, J. A. Rodriguez-Rivera, Y. Qiu, B. Winn, R. J. Cava, and C. L. Broholm, Continuum of quantum fluctuations in a three-dimensional $s = 1$ Heisenberg magnet, *Nat. Phys.* **15**, 54 (2019).
- [24] B. Gao, T. Chen, D. W. Tam, C.-L. Huang, K. Sasmal, D. T. Adroja, F. Ye, H. Cao, G. Sala, M. B. Stone, C. Baines, J. A. T. Verezhak, H. Hu, J.-H. Chung, X. Xu, S.-W. Cheong, M. Nallaiyan, S. Spagna, M. B. Maple, A. H. Nevidomskyy, E. Morosan, G. Chen, and P. Dai, Experimental signatures of a three-dimensional quantum spin liquid in effective spin-1/2 Ce₂Zr₂O₇ pyrochlore, *Nat. Phys.* **15**, 1052 (2019).
- [25] X.-G. Wen, Quantum orders and symmetric spin liquids, *Phys. Rev. B* **65**, 165113 (2002).
- [26] V. Kalmeyer and R. B. Laughlin, Equivalence of the resonating-valence-bond and fractional quantum Hall states, *Phys. Rev. Lett.* **59**, 2095 (1987).
- [27] W. Kadow, L. Vanderstraeten, and M. Knap, Hole spectral function of a chiral spin liquid in the triangular lattice hubbard model, *Phys. Rev. B* **106**, 094417 (2022).
- [28] X.-T. Zhang, Y. Huang, H.-Q. Wu, D. N. Sheng, and S.-S. Gong, Chiral spin liquid and quantum phase diagram of spin- $\frac{1}{2}$ J_1 - J_2 - J_χ model on the square lattice, *Phys. Rev. B* **109**, 125146 (2024).
- [29] Z. Zhu, Chiral spin liquid versus mott antiferromagnetism in the triangular-lattice hubbard model, *Phys. Rev. B* **110**, L041113 (2024).
- [30] B. Bauer, L. Cincio, B. P. Keller, M. Dolfi, G. Vidal, S. Trebst, and A. W. W. Ludwig, Chiral spin liquid and emergent anyons in a kagome lattice mott insulator, *Nat. Commun.* **5**, 5137 (2014).
- [31] Y. Huang, X.-Y. Dong, D. N. Sheng, and C. S. Ting, Quantum phase diagram and chiral spin liquid in the extended spin- $\frac{1}{2}$ honeycomb xy model, *Phys. Rev. B* **103**, L041108 (2021).
- [32] D. Lozano-Gómez, Y. Iqbal, and M. Vojta, A classical chiral spin liquid from chiral interactions on the pyrochlore lattice, *Nat. Commun.* **15**, 10162 (2024).
- [33] A. Fancelli, R. Flores-Calderón, O. Benton, B. Lake, R. Moessner, and J. Reuther, Fragile spin liquid in three dimensions, *Phys. Rev. B* **111**, 134413 (2025).
- [34] H. Yan, O. Benton, R. Moessner, and A. H. Nevidomskyy, Classification of classical spin liquids: Typology and resulting landscape, *Phys. Rev. B* **110**, L020402 (2024).
- [35] N. Niggemann, M. Hering, and J. Reuther, Classical spiral spin liquids as a possible route to quantum spin liquids, *J. Condens. Matter Phys.* **32**, 024001 (2019).
- [36] S. V. Isakov, K. Gregor, R. Moessner, and S. L. Sondhi, Dipolar spin correlations in classical pyrochlore magnets, *Phys. Rev. Lett.* **93**, 167204 (2004).
- [37] C. Castelnovo, R. Moessner, and S. Sondhi, Spin ice, fractionalization, and topological order, *Annu. Rev. Condens. Matter Phys.* **3**, 35 (2012).
- [38] I. Živković, V. Favre, C. Salazar Mejia, H. O. Jeschke, A. Magrez, B. Dabholkar, V. Nocolak, R. S. Freitas, M. Jeong, N. G. Hegde, L. Testa, P. Babkevich, Y. Su, P. Manuel, H. Luetkens, C. Baines, P. J. Baker, J. Wosnitza, O. Zaharko, Y. Iqbal, J. Reuther, and H. M. Rønnow, Magnetic field induced quantum spin liquid in the two coupled trillium lattices of K₂Ni₂(SO₄)₃, *Phys. Rev. Lett.* **127**, 157204 (2021).
- [39] J. M. Hopkinson and H.-Y. Kee, Geometric frustration inherent to the trillium lattice, a sublattice of the B20 structure, *Phys. Rev. B* **74**, 224441 (2006).
- [40] K. Boya, K. Nam, K. Kargeti, A. Jain, R. Kumar, S. K. Panda, S. M. Yusuf, P. L. Paulose, U. K. Voma, E. Kermarrec, K. H. Kim, and B. Koteswararao, Signatures of spin-liquid state in a 3D frustrated lattice compound K₂Fe₂(PO₄)₃ with $S = 5/2$, *APL Materials* **10**, 101103 (2022).

- [41] M.-H. Li, S. Biswas, and S. A. Parameswaran, [Classification of spin-1/2 fermionic quantum spin liquids on the trillium lattice](#) (2024), [arXiv:2409.02898 \[cond-mat.str-el\]](#).
- [42] M. G. Gonzalez, V. Nocolak, A. Sharma, V. Favre, J.-R. Soh, A. Magrez, R. Bewley, H. O. Jeschke, J. Reuther, H. M. Rønnow, Y. Iqbal, and I. Živković, Dynamics of $\text{K}_2\text{Ni}_2(\text{SO}_4)_3$ governed by proximity to a 3D spin liquid model, [Nat. Commun.](#) **15**, 7191 (2024).
- [43] J. Khatua, S. Lee, G. Ban, M. Uhlarz, G. S. Murugan, R. Sankar, K.-Y. Choi, and P. Khuntia, Magnetism and spin dynamics of the $s=\frac{3}{2}$ frustrated trillium lattice compound $\text{K}_2\text{CrTi}(\text{PO}_4)_3$, [Phys. Rev. B](#) **109**, 184432 (2024).
- [44] W. Yao, Q. Huang, T. Xie, A. Podlesnyak, A. Brington, C. Xing, R. S. D. Mudiyansele, H. Wang, W. Xie, S. Zhang, M. Lee, V. S. Zapf, X. Bai, D. A. Tennant, J. Liu, and H. Zhou, Continuous spin excitations in the three-dimensional frustrated magnet $\text{K}_2\text{Ni}_2(\text{SO}_4)_3$, [Phys. Rev. Lett.](#) **131**, 146701 (2023).
- [45] L. Kubíčková, A. K. Weber, M. Panthöfer, S. Calder, and A. Möller, $\text{Cs}_2\text{Fe}_2(\text{MoO}_4)_3$ a strongly frustrated magnet with orbital degrees of freedom and magnetocaloric properties, [Chem. Mat.](#) **36**, 7016 (2024).
- [46] R. Kolay, Q.-P. Ding, Y. Furukawa, A. A. Tsirlin, and R. Nath, Magnetic properties of the double trillium lattice antiferromagnet $\text{KBaCr}_2(\text{PO}_4)_3$, [Phys. Rev. B](#) **110**, 224405 (2024).
- [47] S. Mühlbauer, B. Binz, F. Jonietz, C. Pfleiderer, A. Rosch, A. Neubauer, R. Georgii, and P. Böni, Skyrmion lattice in a chiral magnet, [Science](#) **323**, 915 (2009).
- [48] I. Mahraj and A. Ptak, [Chiral phononic and electronic edge modes of EuPtSi](#) (2024), [arXiv:2409.12807 \[cond-mat.mtrl-sci\]](#).
- [49] T. E. Redpath and J. M. Hopkinson, Spin ice on the trillium lattice studied by monte carlo calculations, [Phys. Rev. B](#) **82**, 014410 (2010).
- [50] S. V. Isakov, J. M. Hopkinson, and H.-Y. Kee, Fate of partial order on trillium and distorted windmill lattices, [Phys. Rev. B](#) **78**, 014404 (2008).
- [51] J. M. Bulled, J. A. M. Paddison, A. Wildes, E. Lhotel, S. J. Cassidy, B. Pato-Doldán, L. C. Gómez-Aguirre, P. J. Saines, and A. L. Goodwin, Geometric frustration on the trillium lattice in a magnetic metal-organic framework, [Phys. Rev. Lett.](#) **128**, 177201 (2022).
- [52] I. V. Zatovsky, M. M. Yatskin, V. N. Baumer, N. S. Slobodyanik, and O. V. Shishkin, Langbeinite-related $\text{K}_2\text{FeSn}(\text{PO}_4)_3$ from single-crystal data, [Acta crystallogr. Section E](#) **63**, i199 (2007).
- [53] See supplementary material for further details on sample synthesis, crystal structure, specific heat, and muon spin relaxation data analysis.
- [54] A. Suter and B. Wojek, Musrfit: A free platform-independent framework for μSR data analysis, [Phys. Procedia](#) **30**, 69 (2012).
- [55] B. H. Toby, [EXPGUI](#), a graphical user interface for [GSAS](#), [J. Appl. Crystallogr.](#) **34**, 210 (2001).
- [56] A. Sen, K. Damle, and R. Moessner, Vacancy-induced spin textures and their interactions in a classical spin liquid, [Phys. Rev. B](#) **86**, 205134 (2012).
- [57] R. Sibille, E. Lhotel, M. Ciomaga Hatnean, G. J. Nilsen, G. Ehlers, A. Cervellino, E. Ressouche, M. Frontzek, O. Zaharko, V. Pomjakushin, U. Stühr, H. C. Walker, D. T. Adroja, H. Luetkens, C. Baines, A. Amato, G. Balakrishnan, T. Fennell, and M. Kenzelmann, Coulomb spin liquid in anion-disordered pyrochlore $\text{Tb}_2\text{Hf}_2\text{O}_7$, [Nat. Commun.](#) **8**, 892 (2017).
- [58] T. Moriya, Anisotropic superexchange interaction and weak ferromagnetism, [Phys. Rev.](#) **120**, 91 (1960).
- [59] P. Svoboda, P. Javorský, M. Diviš, V. Sechovský, F. Honda, G. Oomi, and A. A. Menovsky, Importance of anharmonic terms in the analysis of the specific heat of UNi_2Si_2 , [Phys. Rev. B](#) **63**, 212408 (2001).
- [60] J. Khatua, M. Gomilšek, K.-Y. Choi, and P. Khuntia, Magnetism and field-induced effects in the $s = 5/2$ honeycomb lattice antiferromagnet $\text{FeP}_3\text{SiO}_{11}$, [Phys. Rev. B](#) **110**, 184402 (2024).
- [61] A. P. Ramirez, B. Hessen, and M. Winklemann, Entropy balance and evidence for local spin singlets in a kagomé-like magnet, [Phys. Rev. Lett.](#) **84**, 2957 (2000).
- [62] J. Khatua, M. Gomilšek, J. C. Orain, A. M. Strydom, Z. Jagličić, C. V. Colin, S. Petit, A. Ozarowski, L. Mangin-Thro, K. Sethupathi, M. S. R. Rao, A. Zorko, and P. Khuntia, Signature of a randomness-driven spin-liquid state in a frustrated magnet, [Communications Physics](#) **5**, 99 (2022).
- [63] S. Lee, S.-H. Do, W.-J. Lee, Y. S. Choi, M. Lee, E. S. Choi, A. P. Reyes, P. L. Kuhns, A. Ozarowski, and K.-Y. Choi, Multistage symmetry breaking in the breathing pyrochlore lattice $\text{Li}(\text{Ga},\text{In})\text{Cr}_4\text{O}_8$, [Phys. Rev. B](#) **93**, 174402 (2016).
- [64] S. Lee, T. Zhu, Y. Oshima, T. Shiroka, C. Wang, H. Luetkens, H. Yang, M. Lü, and K.-Y. Choi, Timescale distributions of spin fluctuations in the $s = 2$ kagome antiferromagnet $\text{CsMn}_3\text{F}_6(\text{SeO}_3)_2$, [Phys. Rev. B](#) **105**, 094439 (2022).
- [65] A. Glamazda, Y. S. Choi, S.-H. Do, S. Lee, P. Lemmens, A. N. Ponomaryov, S. A. Zvyagin, J. Wosnitza, D. P. Sari, I. Watanabe, and K.-Y. Choi, Quantum criticality in the coupled two-leg spin ladder $\text{Ba}_2\text{CuTeO}_6$, [Phys. Rev. B](#) **95**, 184430 (2017).
- [66] A. Le Yaouanc and P. D. De Reotier, *Muon spin rotation, relaxation, and resonance: applications to condensed matter*, 147 (OUP Oxford, 2011).
- [67] Y. J. Uemura, T. Yamazaki, D. R. Harshman, M. Senba, and E. J. Ansaldo, Muon-spin relaxation in AuFe and CuMn spin glasses, [Phys. Rev. B](#) **31**, 546 (1985).
- [68] Y. Cai, M. N. Wilson, A. M. Hallas, L. Liu, B. A. Frandsen, S. R. Dunsiger, J. W. Krizan, R. J. Cava, O. Rubel, Y. J. Uemura, and G. M. Luke, μSR study of spin freezing and persistent spin dynamics in $\text{NaCaNi}_2\text{F}_7$, [J. Phys. Condens. Matter.](#) **30**, 385802 (2018).
- [69] Y. J. Uemura, A. Keren, K. Kojima, L. P. Le, G. M. Luke, W. D. Wu, Y. Ajiro, T. Asano, Y. Kuriyama, M. Mekata, H. Kikuchi, and K. Kakurai, Spin fluctuations in frustrated kagomé lattice system $\text{SrCr}_3\text{Ga}_4\text{O}_{19}$ studied by muon spin relaxation, [Phys. Rev. Lett.](#) **73**, 3306 (1994).
- [70] N. Kanazawa, Y. Onose, T. Arima, D. Okuyama, K. Ohoyama, S. Wakimoto, K. Kakurai, S. Ishiwata, and Y. Tokura, Large topological hall effect in a short-period helimagnet MnGe , [Phys. Rev. Lett.](#) **106**, 156603 (2011).
- [71] S.-H. Do, W.-J. Lee, S. Lee, Y. S. Choi, K.-J. Lee, D. I. Gorbunov, J. Wosnitza, B. J. Suh, and K.-Y. Choi, Short-range quasistatic order and critical spin correlations in $\alpha\text{-Ru}_{1-x}\text{Ir}_x\text{Cl}_3$, [Phys. Rev. B](#) **98**, 014407 (2018).
- [72] C. Peng and L. Zhang, Scaling and data collapse of two-dimensional random singlet states in a magnetic field, [Phys. Rev. B](#) **111**, 014409 (2025).

- [73] W. Hong, L. Liu, C. Liu, X. Ma, A. Koda, X. Li, J. Song, W. Yang, J. Yang, P. Cheng, H. Zhang, W. Bao, X. Ma, D. Chen, K. Sun, W. Guo, H. Luo, A. W. Sandvik, and S. Li, Extreme suppression of antiferromagnetic order and critical scaling in a two-dimensional random quantum magnet, *Phys. Rev. Lett.* **126**, 037201 (2021).
- [74] T. Shimokawa, S. Sabharwal, and N. Shannon, [Can experimentally-accessible measures of entanglement distinguish quantum spin liquids from disorder-driven "random singlet" phases ?](#) (2025), arXiv:2505.11874 [cond-mat.str-el].
- [75] C. Lee, S. Lee, H.-S. Kim, S. Kittaka, Y. Kohama, T. Sakakibara, K. H. Lee, J. van Tol, D. I. Gorbunov, S.-H. Do, S. Yoon, A. Berlie, and K.-Y. Choi, Random singlets in the $s = 5/2$ coupled frustrated cubic lattice $\text{Lu}_3\text{Sb}_3\text{Mn}_2\text{O}_{14}$, *Phys. Rev. B* **107**, 214404 (2023).
- [76] A. Silverman and J. Adler, Site-percolation threshold for a diamond lattice with diatomic substitution, *Phys. Rev. B* **42**, 1369 (1990).
- [77] R. Moessner and J. T. Chalker, Low-temperature properties of classical geometrically frustrated antiferromagnets, *Phys. Rev. B* **58**, 12049 (1998).
- [78] E. Kermarrec, R. Kumar, G. Bernard, R. Hénaff, P. Mendels, F. Bert, P. L. Paulose, B. K. Hazra, and B. Koteswararao, Classical spin liquid state in the $s = \frac{5}{2}$ Heisenberg kagome antiferromagnet $\text{Li}_9\text{Fe}_3(\text{P}_2\text{O}_7)_3(\text{PO}_4)_2$, *Phys. Rev. Lett.* **127**, 157202 (2021).
- [79] K.-Y. C. J. Khatua and J. A. Krieger, PSI μSR experiment database, <http://musruser.psi.ch/cgi-bin/SearchDB.cgi>, accessed: [28/06/2025].